Available online at www.sciencedirect.com

ScienceDirect

journal homepage: www.elsevier.com/locate/he

Flame front structure of turbulent premixed flames of syngas oxyfuel mixtures

Meng Zhang [a], Jinhua Wang [a,*], Jin Wu [a], Zhilong Wei [a], Zuohua Huang [a,*], Hideaki Kobayashi [b]

[a] State Key Laboratory of Multiphase Flow in Power Engineering, Xi'an Jiaotong University, Xi'an 710049, PR China
[b] Institute of Fluid Science, Tohoku University, Sendai, Miyagi 980-8577, Japan

ARTICLE INFO

Article history:
Received 23 November 2013
Received in revised form
7 January 2014
Accepted 8 January 2014
Available online 18 February 2014

Keywords:
Syngas oxyfuel combustion
Turbulent burning velocity
Flame front structure
Flame surface density
OH-PLIF

ABSTRACT

In order to investigate oxyfuel combustion characteristics of typical composition of coal gasification syngas connected to CCS systems. Instantaneous flame front structure of turbulent premixed flames of $CO/H_2/O_2/CO_2$ mixtures which represent syngas oxyfuel combustion was quantitatively studied comparing with CH_4/air and syngas/air flames by using a nozzle-type Bunsen burner. Hot-wire anemometer and OH-PLIF were used to measure the turbulent flow and detect the instantaneous flame front structure, respectively. Image processing and statistical analyzing were performed using the Matlab Software. Flame surface density, mean progress variable, local curvature radius, mean flame volume, and flame thickness, were obtained. Results show that turbulent premixed flames of syngas possess wrinkled flame front structure which is a general feature of turbulent premixed flames. Flame surface density for the $CO/H_2/O_2/CO_2$ flame is much larger than that of $CO/H_2/O_2$/air and CH_4/air flames. This is mainly caused by the smaller flame intrinsic instability scale, which would lead to smaller scales and less flame passivity response to turbulence presented by Markstain length, which reduce the local flame stretch against turbulence vortex. Peak value of Possibility Density Function (PDF) distribution of local curvature radius, R, for $CO/H_2/O_2/CO_2$ flames is larger than those of $CO/H_2/O_2$/air and CH_4/air flames at both positive and negative side and the corresponding R of absolute peak PDF is the smallest. This demonstrates that the most frequent scale is the smallest for $CO/H_2/O_2/CO_2$ flames. Mean flame volume of $CO/H_2/O_2/CO_2$ flame is smaller than that of CH_4/air flame even smaller than that of $CO/H_2/O_2$/air flame. This would be due to the lower flame height and smaller flame wrinkles.

1. Introduction

Integrated Gasification Combined Cycle (IGCC) technology has the attractive features due to its particular advantages such as fuel diversity and suitability for Carbon Capture and Storage (CCS) [1,2]. For IGCC power plant, the coal or other fuel resources are gasified and the derived gas is called syngas which is mainly composed of CO and H_2. One of the most superior advantages of IGCC technology is that it can realize near zero CO_2 emissions [3] when it is extended to CCS. The syngas from this system can be applied to the oxyfuel combustion where fuel is burned in oxygen rather than air with recycled flue gas and it is viewed as a new combustion concept [4,5]. Oxyfuel combustion has some attractive merits such as enhanced

* *Corresponding authors*. Fax: +86 29 82668789.
E-mail addresses: jinhuawang@mail.xjtu.edu.cn (J. Wang), zhhuang@mail.xjtu.edu.cn (Z. Huang).
0360-3199/$ – see front matter
http://dx.doi.org/10.1016/j.ijhydene.2014.01.038

Nomenclature

A	area of the burner outlet, mm^2
$< c >$	mean progress variable
c	progress variable
I_0	mean stretch factor
L_M	Markstein length, mm
Le_{eff}	effective Lewis number
l_K	Kolmogorov microscale, mm
l_λ	Taylor microscale, mm
l_0	Integral scale, mm
l_i	flame intrinsic instability scale, mm
Ma	Markstein number
R	local curvature radius, mm
R_{ave}	averaged curvature radius, mm
R^*	critical curvature radius, mm
Re_λ	turbulence Reynolds number based on Taylor microscale
S_L	laminar burning velocity, cm/s
S_{Lk}	local burning velocity for the stretched flame, cm/s
S_T	turbulent burning velocity, cm/s
T_{ad}	adiabatic flame temperature, K
U	mean velocity of the mixtures at the burner outlet, m/s
u'	turbulence intensity, m/s
V_f	mean flame volume, mm^3
$< W >$	mean fuel consumption rate, $kg/(m^3\ s)$
Δx	increment of x of the edge curve
Y_f	mass fraction of the fuel
y', y''	first and second derivative of the edge curve
α_D	thermal diffusivity coefficient, cm^2/s
ϕ	equivalence ratio
θ	angle of the contour $< c >= 0.1$
ε_i	fractal inner cutoff, mm
ν	kinematic viscosity, cm^2/s
ρ_b, ρ_u	burned and unburned mixture density kg/m^3
Σ	flame surface density, mm^{-1}
$< \omega >$	mean reaction rate
δ_L	flame thickness, mm
δ_T	flame brush thickness, mm

radiation heat transfer, downsizing of combustors and free NO_x emissions. With the pure oxygen as the oxidizer, there is nearly no NO_x formation in the combustion process. The concentration of CO_2 in the exhaust gases is relatively high and is much suitable for CCS. Thus, the oxyfuel combustion is an acceptable and promising technique for various highly efficient combustors and systems. In the case of premixed type combustion of IGCC with CCS, the mixture needs to be diluted with recycled flue gas, which contains relatively high concentration of CO_2 to adjust the flame temperature due to its larger heat capacity. Compared to conventional hydrocarbons, both the mixture properties and laminar flame parameters of syngas, i.e. mass diffusivity, laminar burning velocity, and turbulence-chemistry interactions of turbulent premixed flames are significantly different. Therefore, turbulent premixed flame characteristics, such as turbulent burning velocity, flame wrinkle scales, flame surface density and fractal features of syngas is much different comparing to that of hydrocarbon fuels. Those flame characteristics reveal the complicated turbulence-flame interaction since those quantitative parameters were used as the interpretation of turbulent flame front structure [6]. Also, they are essential to the combustion modeling and highly intensive combustor design.

Flame characteristics [7–9] and flame instability [10] of CO/H_2 and CH_4 have been studied on spherical flame laminar Bunsen burner [11] in previous work of the authors' group. They also have been studied by other researches at high pressure [12,13], but the turbulent flow was not involved. However, most of the previous works focused on the syngas/air mixtures and few researches were conducted on the syngas oxyfuel combustion, especially under the turbulent condition. The previous researches of turbulent premixed combustion also have been performed in combustion chamber [14,15], Bunsen burner [16–18] and V shape flames [19] on methane/air flame and limited report on the syngas flames. Furthermore, detailed information of flame front structure is indispensable for flame characterization, although some characteristics were obtained [20–22]. The understanding on detailed flame front structure was not well quantitatively interpreted and flame properties and flow structures were not clarified yet.

On the other hand, turbulent combustion involves multiple processes of vastly different scales. This is manifested by complex flame front structures such as wrinkled flames, flamelets, and flame brushes [6]. Turbulent flame front structure possesses wrinkles of negative curvature surrounding by large pockets of modest positive curvature, which is mainly due to the key pathways of governing reactions under turbulent condition and they significantly differ to those under the laminar condition.

The objective of this study is to declare the turbulence-flame interaction by analyzing turbulent premixed flame front structure of $CO/H_2/O_2$ highly diluted with CO_2. A $CO/H_2/O_2/CO_2$ mixture, whose mole fraction of CO_2 was 0.55 in the whole mixture, was investigated as a model mixture for the typical composition of coal gasification syngas. Turbulence measurements by hot-wire anemometer and OH-PLIF for the turbulent premixed flames were performed to describe the flow field and instantaneous flame front structure. Through OH-PLIF image processing, turbulent burning velocity, flame surface density, local curvature radius distribution and averaged curvature radius, fractal inner cutoff, mean flame volume and flame brush thickness were obtained. The laminar flame parameters were also used to interpret the different phenomenon of flame-turbulence interaction.

2. Experimental procedures and image processing method

2.1. *Experimental setup and parameters calculation method*

The turbulent flame experimental apparatus includes air supply system, turbulent Bunsen burner and OH-PLIF system

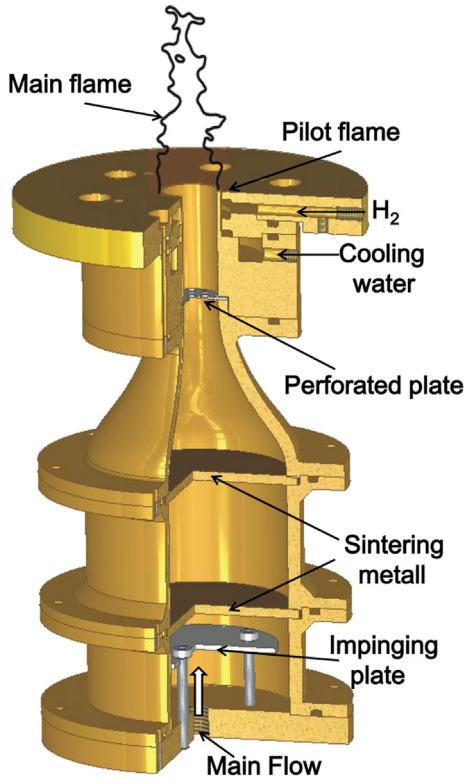

Fig. 1 – The schematic of turbulent premixed Bunsen burner.

[17]. OH-PLIF was verified as good qualitative marker of flame front. The copper nozzle-type turbulent premixed Bunsen burner was used with an outlet diameter of 20 mm to stabilize the flame, as shown in Fig. 1. An impinging plate and two pieces of sintering metal were used to get well mixed fuel–air mixture and rectify the flow. Three kinds of perforated plate were installed 40 mm upstream of the nozzle outlet to generate wide range of turbulence conditions. The orifice diameters are 2.1, 3.4 and 4.0 mm, respectively. A hydrogen diffusion flame was formed around the nozzle outlet as a pilot flame to support the stable flame and the nozzle is water cooled. The details about the experimental setup were described elsewhere [11,17].

The composition and properties of the tested mixtures in this study are summarized in Table 1. The composition of the model coal gasification syngas and equivalence ratio, ϕ, were determined based on previous reports which indicated the major components are CO, H_2 and other gases [23]. In this study, CO_2 concentration of 55% was chosen for the clarification of the combustion characteristics of model syngas oxy-fuel combustion. $CO/H_2/CO_2$/air and CH_4/air mixtures were also introduced for the comparative study. For convenience, the $CO/H_2/CO_2/O_2$ is indicated as CHO, and $CO/H_2/CO_2$/air and CH_4/air are indicated as CHA and CH4, respectively.

The properties of the tested mixtures are summarized in Table 2. The laminar burning velocity S_L, and adiabatic temperature, T_{ad}, were estimated by using the PREMIX code [24] and CHEMKIN-II database [25] with GRI-Mech 3.0 mechanism [26]. S_L for the three mixtures was adjusted approximately identical in this study. The effective Lewis number, Le_{eff}, which represents the diffusional-thermal instability, was calculated by the method of Dinkelacker et al. [27]. It is based on the diffusion coefficient of multicomponent fuel and oxidizer considering stoichiometry. Markstein length, L_M, is an important parameter to describe the stretch effect and understand the turbulent flame characteristics. $L_M = \delta_L Ma$ is used to estimate L_M, where δ_L and Ma are laminar flame thickness and Markstein number, respectively. The characteristic flame instability scale, l_i, which is considered as a dominant factor for the smallest flame wrinkles [16], was calculated by Bechtold and Matalon [28] and Yuan et al. [29] and is also listed in Table 2. It was calculated corresponding to the maximum growth rate in a dispersion relation.

Turbulence parameters were measured using a constant-temperature hot-wire anemometer (Dantec, Streamline 90N) at the center and 1 mm above the burner outlet. The turbulence measure sampling rate is 300 kHz for 5 s. The mean size of the large eddies in a turbulent flow, integral scale, l_0, is evaluated by integrating the correlation coefficient for the fluctuating velocities under the assumption of Taylor's hypothesis and isotropy of the turbulence. Transverse Taylor's microscale, l_λ, related to the mean rate of strain, was calculated to evaluate the turbulence Reynolds number, Re_λ combined with kinematic viscosity, ν. Turbulence scales and turbulence Reynolds number at $u'/S_L \approx 1.45$ are given in Table 3 by fitting the measured value within the experimental range. Fractal inner cutoffs, ε_i, for the tested mixtures calculated with fractal theory by circle method at $u'/S_L \approx 1.45$ are also given in Table 3. Fig. 2 shows the turbulent premixed flames of the present work in the Peters modified Borghi's diagram. It can be seen that most of the flames in the present study locate in the flamelet regime. Thus the flame characteristics can be discussed by assuming flamelet regime.

The instantaneous flame front structure was detected by OH-PLIF measurement as shown in Fig. 3. An Nd:YAG laser (Quanta-Ray Pro-190) with the wavelength of 355 nm and a pumped dye laser (Sirah PRSC-G-3000) with a frequency doubler were used as the laser source. The YAG laser with power of 3 W operated at 10 Hz and pulse time of 10 ns was transferred to the wavelength of 282.769 nm by the dye laser which is used to excite the Q1(8) line of the $A2\Sigma \leftarrow X2\Pi(1,0)$ bands for the OH excitation. The OH fluorescence from the (0, 0) band at wavelength around 308 nm was detected by an ICCD

Table 1 – Summary of the definition and mole fraction of the mixtures.

Mixture	Components	ϕ	X_{CH_4}	X_{H_2}	X_{CO}	X_{N_2}	X_{O_2}	X_{CO_2}
CH4	CH_4/air	0.85	0.082	–	–	0.725	0.193	–
CHA	$CO/H_2/CO_2$/air	0.7	–	0.072	0.134	0.557	0.148	0.089
CHO	$CO/H_2/CO_2/O_2$	1.0	–	0.105	0.195	–	0.150	0.550

Table 2 – Laminar flame properties for the three mixtures in this study.

Mixture	S_L (cm/s)	T_{ad}	Le_{eff}	δ_L (mm)	L_M (mm)	l_i	ν (cm^2/s)
CH4	30.97	2166.7	0.959	0.073	0.261	1.599	0.1606
CHA	29.50	2117.2	0.607	0.091	0.234	1.111	0.1579
CHO	30.70	2578.8	0.546	0.075	0.145	0.614	0.1160

camera through a UV lens (Nikon Rayfact PF 10545MF-UV) with intensified Relay Optics (Lavision VC08-0094) and OH bandpass filter (LaVision VZ08-0222). A 67 × 50 mm^2 region was focused onto the monitor with resolution of 800 × 600 pixels. 500 images was analyzed for deciding mean progress variable, $< c >$, calculating the turbulent burning velocity, S_T, flame surface density, Σ, local curvature radius, R, mean flame volume, V_f and flame brush thickness, δ_T.

2.2. *Image processing method*

For each condition, 500 instantaneous OH-PLIF images were processed for the statistical analysis. The OH-PLIF image was filtered to remove the pixel noise and then binarized, as shown in Fig. 4(a). The threshold value used here was chosen based on the pixel intensity over the whole image. Flame contour was extracted and flame brush was obtained, as shown in Fig. 4(b) and (c). The progress variable, c, indicates the temperature or mass fraction, which $c = 0$ in unburned gas and $c = 1$ in burned gas, was determined. Mean progress variable, $< c >$, was thereby obtained from 500 images superimposing as shown in Fig. 4(d). Turbulent burning velocity, S_T, was calculated by the conventional angle method,

$$S_T = U \sin(\theta/2) \tag{1}$$

where U is the mean velocity at burner exit, θ represents the flame cone of $< c >= 0.1$.

The flame local curvature radius, R, and its statistical properties such as PDF (Probability Density Function) are usually used to describe the wrinkled flame front structure. PDF distribution of R can be used to quantitatively indicate the flame front wrinkles and structure. When flame edge is tracked from original OH-PLIF image, the pixels on the flame edge curve are then considered as the discretized coordinates, regarding the rows and columns of image matrix elements as x and y. In this study, R is calculated by,

$$R = \frac{(1 + y'^2)^{3/2}}{y''} \tag{2}$$

where y' and y'' are the first and second derivative of the edge curve in the measured plane. Those derivatives were calculated by numerically differentiating the coordinates of the flame edge with the interval of 8 pixels on the edge with truncation error of Δx^4. About 280 edges were successfully processed to calculate the curvature radius distribution at each condition. R is defined as positive value when flame front is convex to the unburned mixture and negative if concave. Once the PDF distribution was determined, the ADF (Accumulated Density Function) was thereby obtained by integrating PDF with interval of 0.5 mm as follows,

$$\mathrm{ADF}(R) = \int_0^R \mathrm{PDF} dR \tag{3}$$

The characteristic average radius, R_{ave}, was defined as the integral average of R from −20 to 20 mm with the interval of 0.5 mm, and it can be considered as the average scale of the flame front. R_{ave} was calculated as follows,

$$R_{ave} = \int_0^{R^*} \mathrm{PDF} dR + \left| \int_{-R^*}^{0} \mathrm{PDF} dR \right| \tag{4}$$

where R^* is 20 mm in this study.

3. Results and discussion

3.1. *OH-PLIF images and turbulent burning velocity*

Fig. 3 shows the typical OH-PLIF images of the three mixtures in this study at $u'/S_L \approx 0.40, 1.45$. It is obvious that all the three flames possess the wrinkled flame front structure which is a general feature of turbulent premixed flames [16,17]. The turbulence characteristics for the three mixtures at $u'/S_L \approx 1.45$ are given in Table 3. Kolmogorov scale, l_K, which wrinkle the flame front, for the $CO/H_2/CO_2/O_2$ flame is smaller and turbulence Reynolds number which relates to turbulence intensity is larger than those of other two mixtures. As the result, the flame front of $CO/H_2/CO_2/O_2$ flame is much finer and wrinkled compared to those of $CO/H_2/CO_2$/air and CH_4/air flames. Deep cusps with small scale are presented in $CO/H_2/CO_2/O_2$ and $CO/H_2/CO_2$/air flames, especially in the former flame. This reveals the higher flame surface density and smaller flame wrinkle scale. At the same u'/S_L, flame height of $CO/H_2/CO_2/O_2$ is decreased due to the smaller turbulence scale and larger turbulence Reynolds number, as shown in Table 3. This reveals the different turbulence-flame interactions among those three mixtures. With increasing u'/S_L, the structure of flame region becomes fine and convoluted in all

Table 3 – Turbulence and flame front characteristics for the tested mixtures at $u'/S_L \approx 1.45$.

Mixture	U (m/s)	u' (m/s)	u'/S_L	l_K (mm)	l_λ (mm)	l_0/δ_L	Re_λ	ε (mm)
CH4	4.39	0.449	1.45	0.1205	0.4330	20.05	43.37	0.9265
CHA	4.09	0.428	1.45	0.1248	0.4127	16.35	42.96	0.7091
CHO	3.94	0.445	1.45	0.0959	1.2225	19.58	46.90	0.6177

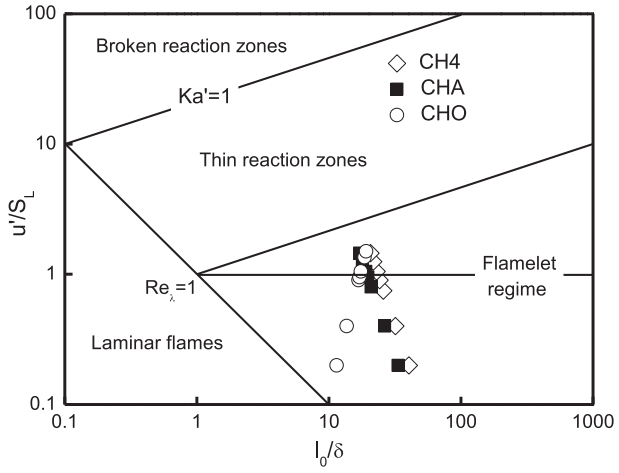

Fig. 2 – Regimes of tested turbulent premixed flames revised by Peters [32].

cases. The fine wrinkled flame structure for the $CO/H_2/CO_2/O_2$ flame is much more distinguished as u'/S_L is increased. In the case of CH_4/air flames, the convoluted front structure also appears, but large scale wrinkles become more frequent and fine scale cusps do not present even at $u'/S_L \approx 1.45$.

Fig. 5 shows the turbulent burning velocity, S_T, normalized by laminar burning velocity, S_L, for $CO/H_2/CO_2/O_2$ flames compared with other two mixtures. Results show that S_T/S_L significantly increases with the increase of u'/S_L. Increasing of u'/S_L induces a large decrease of small turbulent scales. As a result, smaller flame surface elements dominate the turbulent flame structure, leading to finer wrinkles or larger flame front area and consequently increase the burning velocity. S_T/S_L for the CHO flames is larger than that of CH4 and CHA flames within the whole experimental range even though S_L is identical for all tested mixtures. This is due to the smaller flame instability scale, l_i, Lewis number, Le_{eff}, and less flame passivity against turbulence represented by L_M. In previous researches [30,31], S_T was figured out to be an ensemble interpretation of turbulent flame front. Thus, the results in this study suggest that syngas oxyfuel combustion is significantly different to other mixtures in flame characteristics and turbulence-flame interaction. The detailed parameters and discussion will be presented in the later sections.

3.2. *Flame surface density*

The flame characteristics were assumed in flamelet regime in this study because most of the conditions locate at flamelet regime of Borghi's diagram revised by Peters [32], as shown in Fig. 2. Under this consideration, a turbulent flame zone is viewed as an ensemble of laminar flamelets and the total burning rate, $< \omega >$, of the flame is consequently the integration of local burning rate over flame surface. Bray [33] has given the expression of $< \omega >$ related to flame surface density, Σ, which can be expressed as,

$$< \omega >= \rho_u S_L I_0 \sum = \rho_u S_{Lk} \sum \quad (5)$$

where $< \omega >$ is the mean reaction rate, ρ_u is density of unburned gas, I_0 is mean stretch factor, and Σ is flame surface density. In this study, Σ was measured by counting the pixels in the interrogation box with the size of 11 × 11 pixel (resolution is about 0.136 mm) at each location of interest [34], assuming the isotropic flame front structure. On the basis of the average of 500 images, the flame surface density field and profiles of flame surface density were obtained.

Fig. 6 shows the flame surface density field and contours of the mean progress variable, $< c >$, of the tested mixtures under the conditions of Fig. 3. Σ well corresponds to the wrinkled structures and flame heights in terms of thickness and flame volume of the turbulent flame region. Compared to the CH4 flames, the syngas flames (CHA and CHO) give higher Σ under both conditions, indicating that large amount of fine wrinkle structure produces higher Σ and larger scale flame wrinkles produce lower Σ. It also can be clearly seen that flame height of CHO is the smallest and that of CHA comes second, while flame height of CH4 is the largest at both $u'/S_L \approx 0.40$ and 1.45. However, the difference of flame height is weak at $u'/S_L \approx 1.45$. Lower flame height leads to smaller mean flame volume and flame brush thickness. Fig. 7 shows the relationship between mean progress variable, $< c >$, and Σ at relevant conditions corresponding to Fig. 6. In all cases, the Σ profiles are approximately quadratic and symmetric. Σ of CHO is significantly larger than that of CH4 flame, even larger than that of CHA due to the enhancement of flame instability

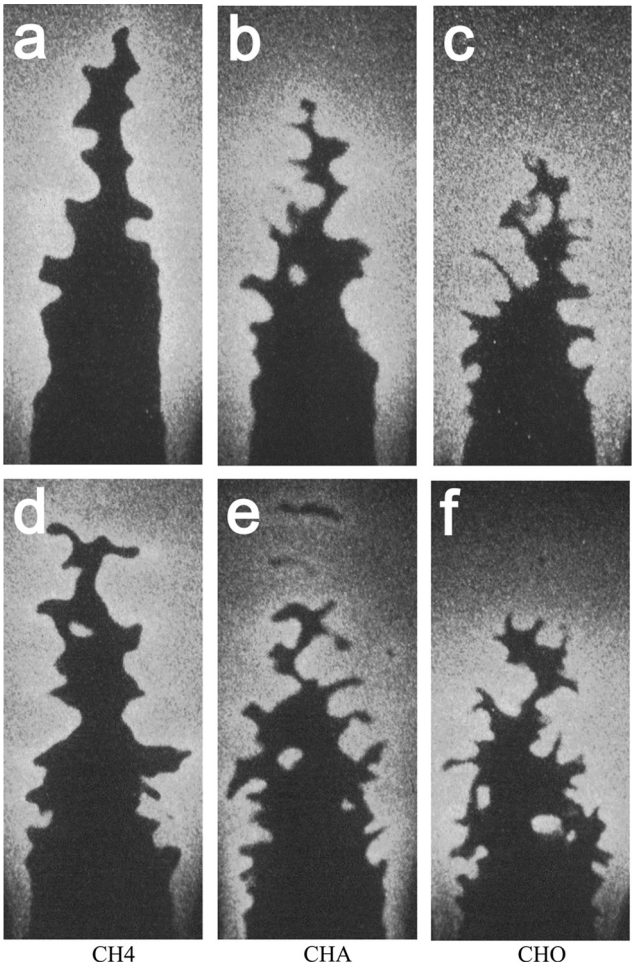

Fig. 3 – OH-PLIF images of the turbulent premixed flames at: a, b, c: $u'/S_L \approx 0.40$; d, e, f: $u'/S_L \approx 1.45$.

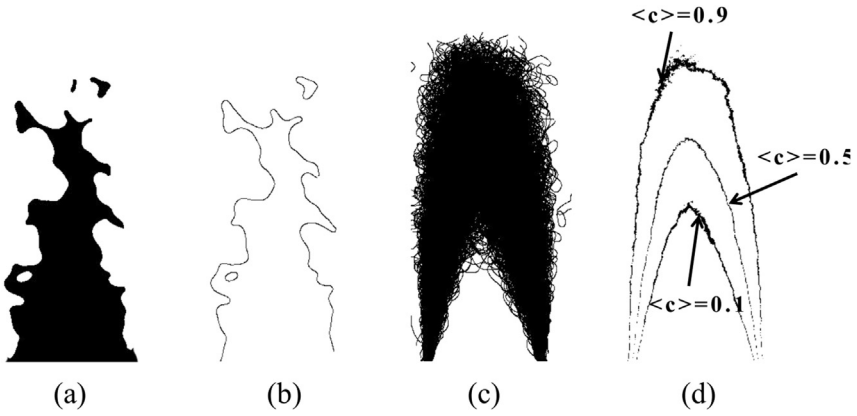

Fig. 4 – Procedures of the image processing to determine the progress variable contour, <c>.

represented by effective Lewis number, Le_{eff}, and flame intrinsic instability scale, l_i, as shown in Table 2. The increase in flame surface density can be attributed to the intensity of wrinkles of flame front and local flame instability. The flame instability scale, l_i, of CH4, CHA and CHO, which can be understood to generate the small scale in the flame, are 1.599, 1.111 and 0.614, respectively. This indicates that flame wrinkles intensity of CHO is the largest of the three mixtures and thus leads to the largest Σ. This can be validated by the local curvature radius distribution and averaged radius as shown in Fig. 8. Local flame instability represented by effective Lewis number, Le_{eff}, decreases in the order of CH4, CHA and CHO, as shown in Table 2. Furthermore, flame thickness, δ_L, calculated by $\delta_L = \alpha_D/S_L$ is another parameter that influences the flame passivity response interpreted by Markstein length, L_M. When L_M is small, flame passivity response which represents local stretch effect caused by turbulent vortex is reduced, leading more small scales and more wrinkled flame front. Thus, Σ of CHO is the largest of the tested mixtures. However, Fig. 7 shows that Σ tends to be slightly smaller at $u'/S_L \approx 1.45$ comparing to that of $u'/S_L \approx 0.40$ and seems to be an inverse tendency because flame wrinkles increases and turbulence scales decrease with turbulence intensity. That would be due to the enhanced flame volume and flame brush thickness in higher turbulence conditions.

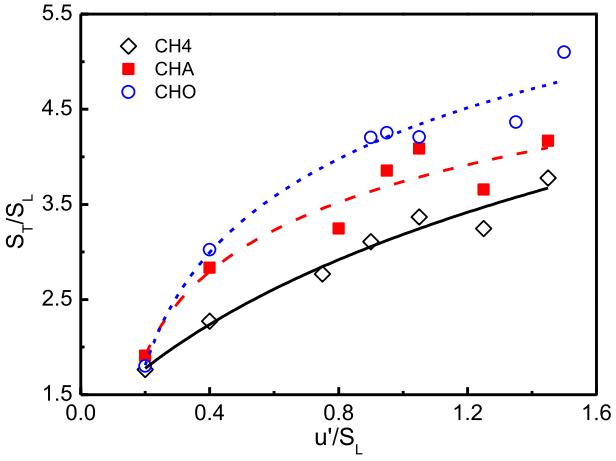

Fig. 5 – Relationship between S_T/S_L and u'/S_L for tested mixtures at various conditions.

3.3. *Local curvature radius distribution*

Fig. 8 shows the distribution of R and R_{ave} of the tested mixtures at $u'/S_L \approx 1.45$. Peak of PDF distribution of R for CHO is higher than that of CH4 and CHA at both positive and negative side and the corresponding R to absolute peak PDF value is smaller. Moreover, the R_{ave} of CHO is the smallest of the three mixtures. This indicates that the most frequent scale of CHO flame front is smaller and this can be validated by the fractal inner cutoffs, ε_i, as shown in Table 3, which is considered as the smallest scale of flame front. The different response of flame wrinkles to turbulence of CHO flame is mainly resulted from the lower effective Lewis number and Markstein length. Production of the smallest scale wrinkles would be attributed to flame instability scale, l_i, which was

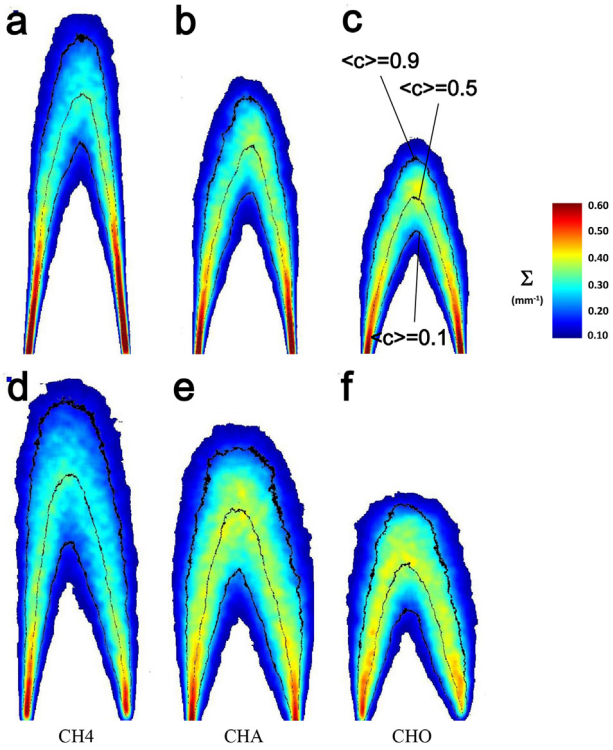

Fig. 6 – Flame surface density, Σ, distribution in the flame brush region at: a, b, c: $u'/S_L \approx 0.40$; d, e, f: $u'/S_L \approx 1.45$.

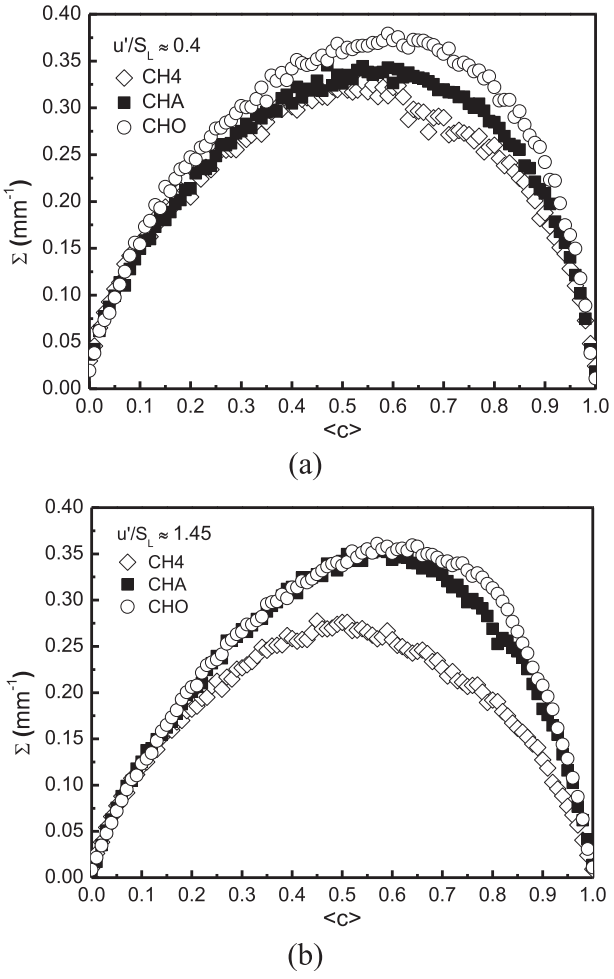

Fig. 7 – Variations of mean progress variable, <c>, and flame surface density, Σ.

also listed in Table 2. For further fractal analysis, the inner cutoff variations versus u'/S_L of the three mixtures in present paper needs to be confirmed in the coming study. The results of PDF distribution of R is used to validate the flame surface density of the tested mixtures in the later section. Moreover, the peak value of PDF distribution of R is not identical for two

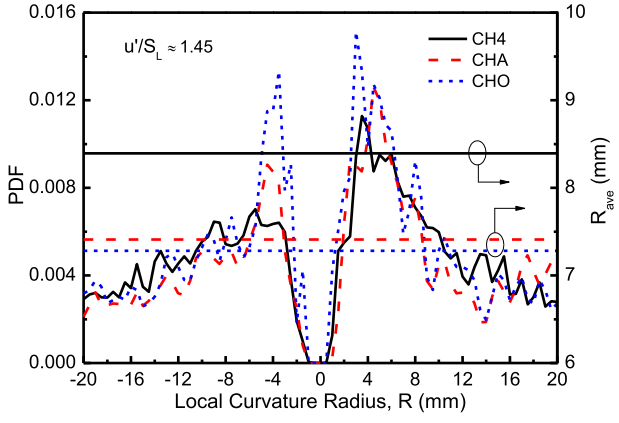

Fig. 8 – PDF distributions of the local curvature radius for the tested mixtures.

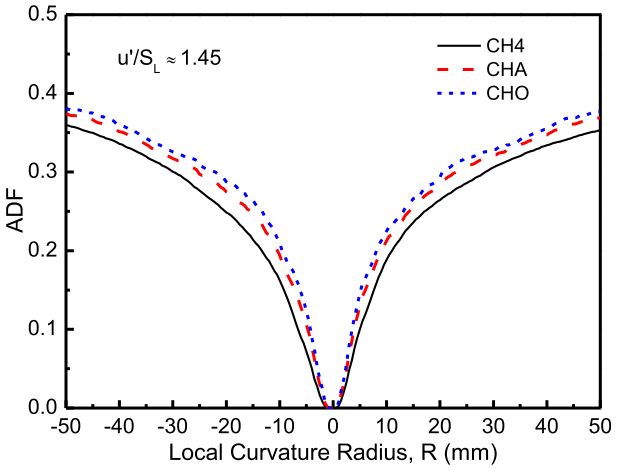

Fig. 9 – Variations of ADF distributions of the local curvature radius for the tested mixtures.

sides and shows an obvious bias to positive radius under all conditions. This indicates that the convex structure to unburned mixture in turbulent flame front is more frequent than that of the concave. The unstable flame characteristic resulting from sub unity Lewis number is responsible for this phenomenon.

Fig. 9 shows the ADF of the local curvature radius for the tested mixtures at $u'/S_L \approx 1.45$. Similar tendency with PDF distribution is also presented. The ADF of CHO flames is larger than that of other two mixtures at both convex and concave structures corresponding to smaller scales of CHO flame structures.

Fig. 10 shows the effect of u'/S_L on R_{ave}. For all the three mixtures, R_{ave} deceases with u'/S_L especially at lower turbulence intensity mainly caused by the turbulence vortex scale decreasing with turbulence intensity. R_{ave} of CHA and CHO gives almost the same and is much smaller than that of CH4. This would be due to the smaller kinetic viscosity, ν, and flame intrinsic instability scale, l_i.

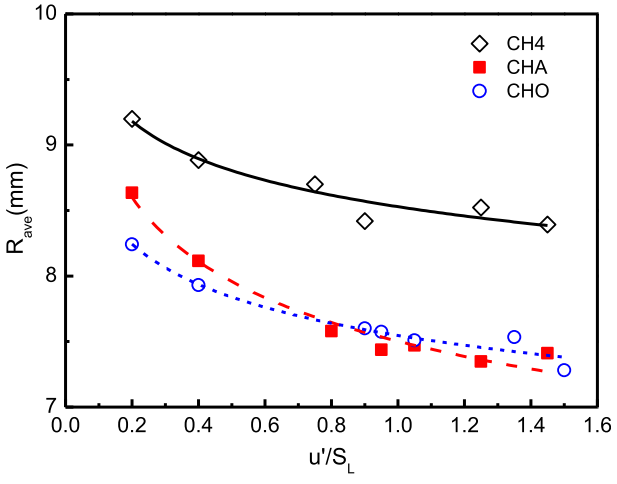

Fig. 10 – Variations of averaged flame local radius, R_{ave}, with u'/S_L.

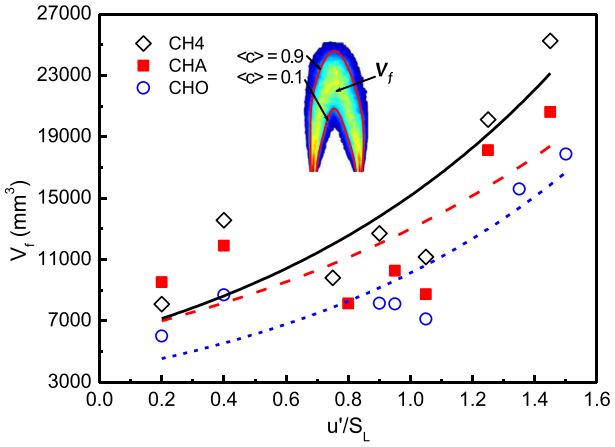

Fig. 11 – Variations of mean flame volume, V_f, with u'/S_L.

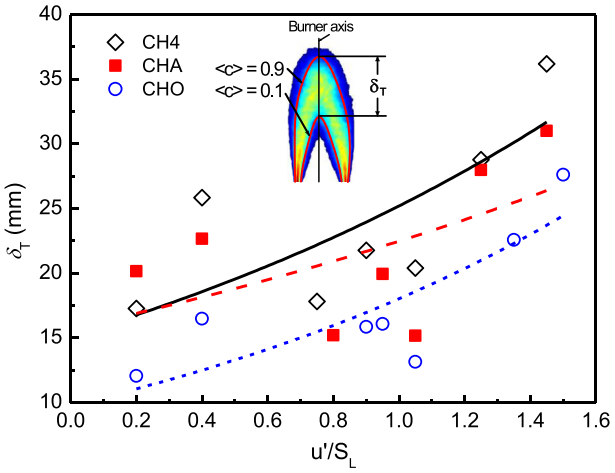

Fig. 12 – Variations of flame brush thickness, δ_T, with u'/S_L.

3.4. *Flame brush thickness and mean flame volume*

Mean flame volume of premixed type flame is an important parameter in turbulent combustion model for connecting to the mean fuel consumption rate, $< W >$, by the following equation,

$$< W >= \rho_u Y_f UA/V_f \quad (6)$$

where ρ_u and Y_f are the density of the mixture and mass fraction of fuel, U is the mean velocity at the burner outlet, and A is the area of the burner outlet. Fig. 11 shows the mean flame volume of the turbulent flame region, V_f, with u'/S_L, which is defined by the space of the region from $< c >= 0.1$ to $< c > = 0.9$ assuming symmetrical flame. The volume was calculated by integrating the region after the polynominal curve for $< c >$ was numerically rotated 360° around the flame center axis. Detailed method was introduced elsewhere [16].

Fig. 11 shows that V_f increases quickly with the increase of u'/S_L. The effect of u'/S_L on V_f are probably caused by the increase in mean velocity and depth of the deep cusps of large scale flame wrinkles. Turbulence intensity is mainly increased by the mean flow velocity at burner exit. This leads to larger fuel consumption and consequently increases the flame height which can result in thicker flame brush and larger mean flame volume. Scale characteristics of turbulent flame front with u'/S_L obtained in the present study can be interpreted on the basis of the depth and scale of the wrinkles. A deep wrinkle of a concave structure refers to unburned mixture penetrating to the main post flame. This is another important factor for the increase of mean flame volume as the increase of u'/S_L. It is clearly seen from Fig. 11 that V_f for CHO flames is smaller than those of CH4 flames even those of CHA under all conditions. This is mainly because of the less flame passivity response and lower flame height for syngas. According to previous research, larger V_f, which also can be viewed as the heat-release region, would extend heat release profile and further restrain combustion oscillation [35]. Thus, the result of V_f implies that syngas oxyfuel combustion has higher possibility to cause combustion oscillation in the premixed type combustion.

The flame brush thickness, δ_T, which indicates the spatial region where the reaction layers are located is very important for the validation of numerical simulations. And it appears to be a meaningful turbulent combustion characteristic as important as turbulent burning velocity for normalizing the progress variable as a universal dimensionless variable of full description of the flame [36]. Fig. 12 shows the relationship of δ_T and u'/S_L. It is clearly seen that δ_T increases quickly with the increase of u'/S_L. The δ_T of CHO flames is the smallest for the three tested mixtures and this is an important factor influencing Σ as shown in previous.

4. Conclusions

To explore the detailed flame front structure and flame-turbulence interaction of the oxyfuel combustion of model syngas, a $CO/H_2/O_2$ mixture highly diluted with CO_2 was experimentally studied. Comparison with $CO/H_2/CO_2$/air and CH_4/air flames were also made. A Turbulent Bunsen burner and OH-PLIF were used to stabilize the flame and detect the instantaneous flame front structure. Quantitative parameters were obtained to interpret the flame front structure. Main conclusions are summarized as follows:

1. Bunsen type turbulent premixed flames of syngas possess wrinkled flame front structure which is a general feature of the turbulent premixed flames. The wrinkles intensity is higher for $CO/H_2/O_2/CO_2$ flames and the smallest wrinkle scale is more remarkable than those of $CO/H_2/O_2$/air and CH_4/air flames. Turbulent burning velocity of CHO flame is larger than the other two mixtures.
2. Flame surface density for the $CO/H_2/O_2/CO_2$ flame is much larger than that of CH_4/air flames. This mainly caused by smaller flame intrinsic instability scale, l_i which would lead to smaller scales and less flame passivity response presented by L_M, which reduce the local flame stretch against turbulence vortex.
3. Peak value of PDF distribution of R for $CO/H_2/O_2/CO_2$ flames is larger than that of $CO/H_2/O_2$/air and CH_4/air flames at both positive and negative side and the R corresponding to

absolute peak PDF gives the smallest for $CO/H_2/O_2/CO_2$ flames. This would be due to the unstable flame characteristic represented by Lewis number and flame intrinsic instability scale, l_i.

4. Mean flame volume of $CO/H_2/O_2/CO_2$ flame is smaller than that of CH_4/air and $CO/H_2/O_2$/air flames due to lower flame height and smaller flame wrinkles. It suggests that CHO would have higher combustion oscillation possibility in premixed type combustor.

Acknowledgments

This study is supported by National Natural Science Foundation of China (Nos. 51376004, 51006080) and Specialized Research Fund for the Doctoral Program of Higher Education (20130201130011). The support from the Fundamental Research Funds for the Central Universities is also appreciated. Jinhua Wang acknowledges the Japan Society for the Promotion of Science for a JSPS Postdoctoral Fellowship grant.

REFERENCES

[1] Longwell J, Rubin E, Wilson J. Coal: energy for the future. Prog Energy Combust Sci 1995;21:269–360.
[2] Wall TF. Combustion processes for carbon capture. Proc Combust Inst 2007;31:31–47.
[3] Buhre B, Elliott L, Sheng C, Gupta R, Wall T. Oxy-fuel combustion technology for coal-fired power generation. Prog Energy Combust Sci 2005;31:283–307.
[4] Wall T, Liu Y, Spero C, Elliott L, Khare S, Rathnam R, et al. An overview on oxyfuel coal combustion – state of the art research and technology development. Chem Eng Res Des 2009;87:1003–16.
[5] Toftegaard MB, Brix J, Jensen PA, Glarborg P, Jensen AD. Oxy-fuel combustion of solid fuels. Prog Energy Combust Sci 2010;36:581–625.
[6] Dagaut P, Egolfopoulos FN. Editorial comment. Combust Flame 2012;159:2531–2.
[7] Wang J, Huang Z, Kobayashi H, Ogami Y. Laminar burning velocities and flame characteristics of $CO–H_2–CO_2–O_2$ mixtures. Int J Hydrogen Energy 2012;37:19158–67.
[8] Hu EJ, Fu J, Pan L, Jiang X, Huang ZH, Zhang Y. Experimental and numerical study on the effect of composition on laminar burning velocities of $H_2/CO/N_2/CO_2$/air mixtures. Int J Hydrogen Energy 2012;37:18509–19.
[9] Hu EJ, Huang ZH, He JJ, Jin C, Zheng JJ. Experimental and numerical study on laminar burning characteristics of premixed methane–hydrogen–air flames. Int J Hydrogen Energy 2009;34:4876–88.
[10] Miao H, Lu L, Huang Z. Flammability limits of hydrogen-enriched natural gas. Int J Hydrogen Energy 2011;36:6937–47.
[11] Fu J, Tang C, Jin W, Thi LD, Huang Z, Zhang Y. Study on laminar flame speed and flame structure of syngas with varied compositions using OH-PLIF and spectrograph. Int J Hydrogen Energy 2013;38:1636–43.
[12] Sivaramakrishnan R, Comandini A, Tranter R, Brezinsky K, Davis S, Wang H. Combustion of CO/H_2 mixtures at elevated pressures. Proc Combust Inst 2007;31:429–37.
[13] Sung C-J, Law CK. Fundamental combustion properties of H_2/CO mixtures: ignition and flame propagation at elevated pressures. Combust Sci Technol 2008;180:1097–116.
[14] Fairweather M, Ormsby MP, Sheppard CGW, Woolley R. Turbulent burning rates of methane and methane–hydrogen mixtures. Combust Flame 2009;156:780–90.
[15] Nakahara M, Shirasuna T, Hashimoto J. Experimental study on local flame properties of hydrogen added hydrocarbon premixed turbulent flames. J Therm Sci Technol 2009;4:190–201.
[16] Zhang M, Wang J, Xie Y, Wei Z, Jin W, Huang Z, et al. Measurement on instantaneous flame front structure of turbulent premixed CH_4/H_2/air flames. Exp Therm Fluid Sci 2014;52:288–96.
[17] Zhang M, Wang J, Xie Y, Jin W, Wei Z, Huang Z, et al. Flame front structure and burning velocity of turbulent premixed CH_4/H_2/air flames. Int J Hydrogen Energy 2013;38:11421–8.
[18] Vreman AW, van Oijen JA, de Goey LPH, Bastiaans RJM. Direct numerical simulation of hydrogen addition in turbulent premixed Bunsen flames using flamelet-generated manifold reduction. Int J Hydrogen Energy 2009;34:2778–88.
[19] Guo HS, Tayebi B, Galizzi C, Escudie D. Burning rates and surface characteristics of hydrogen-enriched turbulent lean premixed methane–air flames. Int J Hydrogen Energy 2010;35:11342–8.
[20] Wang JH, Matsuno F, Okuyama M, Ogami Y, Kobayashi H, Huang ZH. Flame front characteristics of turbulent premixed flames diluted with CO_2 and H_2O at high pressure and high temperature. Proc Combust Inst 2013;34:1429–36.
[21] Bell JB, Day MS, Grcar JF, Lijewski MJ, Driscoll JF, Filatyev SA. Numerical simulation of a laboratory-scale turbulent slot flame. Proc Combust Inst 2007;31:1299–307.
[22] Lachaux T, Halter F, Chauveau C, Gökalp I, Shepherd IG. Flame front analysis of high-pressure turbulent lean premixed methane–air flames. Proc Combust Inst 2005;30:819–26.
[23] Ichikawa Y, Otawara Y, Kobayashi H, Ogami Y, Kudo T, Okuyama M, et al. Flame structure and radiation characteristics of $CO/H_2/CO_2$/air turbulent premixed flames at high pressure. Proc Combust Inst 2011;33:1543–50.
[24] Kee RJ, Grcar JF, Smooke MD, Miller JA, Meeks E. A program for modeling steady, laminar, one-dimensional premixed flames. Albuquerque, NM: Sandia National Laboratories; 1985.
[25] Kee RJ, Rupley FM, Meeks E, Miller JA. A fortran chemical kinetics package for the analysis of gas-phase chemical and plasma kinetics. Albuquerque, NM: Sandia National Laboratories; 1993.
[26] Gregory P, Smith DM, Frenklach Michael, Moriarty Nigel W, Eiteneer Boris, Goldenberg Mikhail, Bowman Thomas C, Hanson Ronald K, Song Soonho, Gardiner Jr William C, Lissianski Vitali V, and Qin Zhiwei 1994.
[27] Dinkelacker F, Manickam B, Muppala SPR. Modelling and simulation of lean premixed turbulent methane/hydrogen/air flames with an effective Lewis number approach. Combust Flame 2011;158:1742–9.
[28] Bechtold JK, Matalon M. The dependence of the Markstein length on stoichiometry. Combust Flame 2001;127:1906–13.
[29] Yuan J, Ju YG, Law CK. On flame-front instability at elevated pressures. Proc Combust Inst 2007;31:1267–74.
[30] Smallwood GJ, Gülder ÖL, Snelling DR, Deschamps BM, Gökalp I. Characterization of flame front surfaces in turbulent premixed methane/air combustion. Combust Flame 1995;101:461–70.
[31] Kobayashi H, Tamura T, Maruta K, Niioka T, Williams FA. Burning velocity of turbulent premixed flames in a high-pressure environment. In: Twenty-sixth symposium 1996. pp. 389–96.

[32] Peters N. Turbulent combustion. Cambridge UK: Cambridge University Press; 2000.
[33] Bray KNC. Studies of the turbulent burning velocity. Proc Royal Soc Lond Ser A Math Phys Sci 1990;431:315–35.
[34] Filatyev SA, Driscoll JF, Carter CD, Donbar JM. Measured properties of turbulent premixed flames for model assessment, including burning velocities, stretch rates, and surface densities. Combust Flame 2005;141:1–21.
[35] Kato S, Fujimori T, Dowling AP, Kobayashi H. Effect of heat release distribution on combustion oscillation. Proc Combust Inst 2005;30:1799–806.
[36] Lipatnikov AN, Chomiak J. Turbulent flame speed and thickness: phenomenology, evaluation, and application in multi-dimensional simulations. Prog Energy Combust Sci 2002;28:1–74.